

**Wiley Analytical Science**

# **Wiley Analytical Science Virtual Conference**

**November 9-17**

## **For the 3rd time, The Wiley Analytical Science Conference is back!**

**It's all happening November 9 - 17**

The Wiley Analytical Science Virtual Conference will bring together thousands of researchers and practitioners to share current developments in science and industry. Join for exciting presentations from experts in the fields of analytical and bioanalytical chemistry, pharmaceutical research, materials science, lab automation, and related disciplines.

Register to learn about recent developments & applications in:

- Microscopy
- Spectroscopy
- Mass Spectrometry
- Separation Science
- Much more!

**Register here**

**WILEY**

# Redox-Mediated Red-Phosphorous Semi-Liquid Anode Enabling Metal-Free Rechargeable Na-Seawater Batteries with High Energy Density

Yongil Kim, Alberto Varzi, Alessandro Mariani, Guk-Tae Kim,\* Youngsik Kim,\* and Stefano Passerini\*

Sodium-seawater batteries (Na-SWB) are considered among the most promising electrochemical devices for large-scale energy storage and the marine sector. In fact, by employing an open-structured cathode, they benefit from the unlimited supply of sodium from seawater. This means, that the energy of such systems is intrinsically limited by the capacity of the anode. In order to increase the energy of Na-SWB, it is therefore necessary to introduce a high-capacity anode such as, e.g., red phosphorus. However, due to its large volume changes upon charge/discharge processes, obtaining thick electrodes and large areal capacity is extremely challenging. Herein, the areal/absolute capacity of the red phosphorus anode is increased by employing a semi-liquid electrode, which includes two redox mediators, i.e., sodium-biphenyl and sodium-pyrene, as reducing and oxidizing species for the exploitation of the full red phosphorus capacity. As a result, the red phosphorus semi-liquid anode in Na-SWB provides a high-capacity of 15 mAh cm<sup>-2</sup> in a static anode, showing great energy storage potential for operation in flow-mode when storing the semi-liquid negative electrode in a storage tank.

is an environmentally friendly energy conversion and storage system employing seawater, one of the most abundant natural resources on earth, as Na-ions source.<sup>[3]</sup> Compared to conventional rechargeable battery chemistries, it also provides improved stability owing to the solid-state electrolyte membrane included in its multilayer electrolyte configuration.<sup>[4]</sup> Additionally, the open-structured cathode design allows for the use of high-capacity alloying/conversion-based anodes, since their initial irreversible capacity does not affect the full-cell performance.<sup>[5]</sup> This is a remarkable advantage of Na-SWB compared with, e.g., conventional lithium-ion batteries (LIB) and sodium-ion batteries (SIB), where the closed system complicates the practical implementation of high-capacity anodes due to the limited Li/Na-ions provided by the cathode. In previous works, an amorphous red phosphorus/carbon (P/C) composite was reported as high-capacity anode material for rechargeable seawater batteries, for the first time.<sup>[6]</sup> The P/C composite has recently been investigated as potential anode material for SIBs too, offering high reversible capacity around 1860 mAh g<sup>-1</sup><sub>phosphorus</sub> (= 1300 mAh g<sup>-1</sup><sub>composite</sub>) in Na-ion half-cell and delivering more than 920 mAh g<sup>-1</sup><sub>composite</sub> over 80 cycles including a good rate capability in Na-SWB.<sup>[6,7]</sup> However, the P/C composite, featuring an alloying/conversion reaction mechanism, suffers from two well-known degradation mechanisms.<sup>[8]</sup> First, the SEI layer cannot entirely withstand the volumetric changes occurring upon repeated charge/discharge. This causes the continuous thickening of the SEI resulting on decreased activity of the P/C composite. Second, the volumetric variations cause loss of continuous electronic paths in the electrode and detachment of the active material from the current collector. Clearly, both these problems make it particularly hard to achieve thick anodes to increase the battery energy density.

Therefore, with the aim of increasing the areal capacity of the P/C composite, two complementary approaches are proposed in this work. The first is the implementation of a semi-solid electrode. This concept is similar to previous works where, e.g., Ketjen black conductive carbon and lithium cobalt oxide powders were shown to have electron connecting networks in the electrolyte.<sup>[9]</sup> The second is the use of redox mediators, i.e., redox active materials with reversible electrochemical behavior and appropriate electrochemical reaction potential, in


## 1. Introduction

Sodium-seawater batteries (Na-SWBs) are being extensively investigated as viable battery technology for application in large-scale energy storage systems (ESS), owing to the abundance and low cost of Na-based raw materials.<sup>[1,2]</sup> In fact, the Na-SWB

Y. Kim, A. Varzi, A. Mariani, G.-T. Kim, S. Passerini  
Helmholtz Institute Ulm (HIU)  
Helmholtzstrasse 11, 89081 Ulm, Germany  
E-mail: guk-tae.kim@kit.edu; stefano.passerini@kit.edu

Y. Kim, A. Varzi, A. Mariani, G.-T. Kim, S. Passerini  
Karlsruhe Institute of Technology (KIT)  
P.O. Box 3640, 76021 Karlsruhe, Germany

Y. Kim  
School of Energy & Chemical Engineering  
Ulsan National Institute of Science and Technology (UNIST)  
UNIST-gil 50, Ulsan 44919, Republic of Korea  
E-mail: ykim@unist.ac.kr

 The ORCID identification number(s) for the author(s) of this article can be found under <https://doi.org/10.1002/aenm.202102061>.

© 2021 The Authors. Advanced Energy Materials published by Wiley-VCH GmbH. This is an open access article under the terms of the Creative Commons Attribution-NonCommercial-NoDerivs License, which permits use and distribution in any medium, provided the original work is properly cited, the use is non-commercial and no modifications or adaptations are made.

DOI: 10.1002/aenm.202102061

the electrolyte to favor the redox reactions of the active material (phosphorus). This concept has been widely developed for lithium-oxygen batteries,<sup>[10,11]</sup> where lithium peroxide is formed upon discharge, which is difficult to be electrochemically recharged. A redox mediator soluble in the electrolyte would be preferentially oxidized and, subsequently, would react with lithium peroxide releasing oxygen gas and, thus, reducing the polarization in lithium-oxygen batteries.<sup>[10]</sup> Combining these two concepts, a semi-liquid anode based on phosphorus and featuring redox mediators was developed. The red phosphorus semi-liquid anode was prepared by mixing the P/C composite powder with a redox mediators-based electrolyte solution. Two polycyclic aromatic hydrocarbons (PAHs) were selected as redox mediators (couples) for the red phosphorus semi-liquid anode.<sup>[12]</sup> In fact, PAHs react with alkali metals (Li, Na, and K) forming alkali metal cations-radical anions complexes. When in contact with sodium (Na) metal, sodium-polycyclic aromatic hydrocarbons (Na-PAHs) are formed. Among them, sodium-biphenyl (Na-BP) has been already studied as liquid anode material for sodium-based batteries, demonstrating high reversibility, low redox potential (vs Na/Na<sup>+</sup>) and suitable electronic and ionic conductivities.<sup>[4,13]</sup> The redox potential of Na-

PAHs has been shown to depend on their structure.<sup>[12]</sup> In our case, Na-BP and sodium-pyrene (Na-PYR) are used as reducing and oxidizing redox mediators for the P/C composite, respectively. Our results demonstrate that the red phosphorus semi-liquid electrode including redox mediators enables high areal capacity anodes for sodium-based batteries and, especially, Na-SWB.

## 2. Results and Discussion

### 2.1. Two Core Motifs

As shown in **Figure 1a**, Na-BP and Na-PYR act as reducing and oxidizing mediators (couples), respectively. The working mechanism of the redox mediators is described in details in **Figure 1b**. When the sodiated red phosphorus is desodiated, a large polarization is normally observed, due to the volumetric changes of the P/C composite and the small contact area between the P/C particles in the dispersion. In the presence of Na-PYR, Na-PYR is firstly desodiated (oxidized) instead. The desodiated PYR then chemically oxidizes the P/C

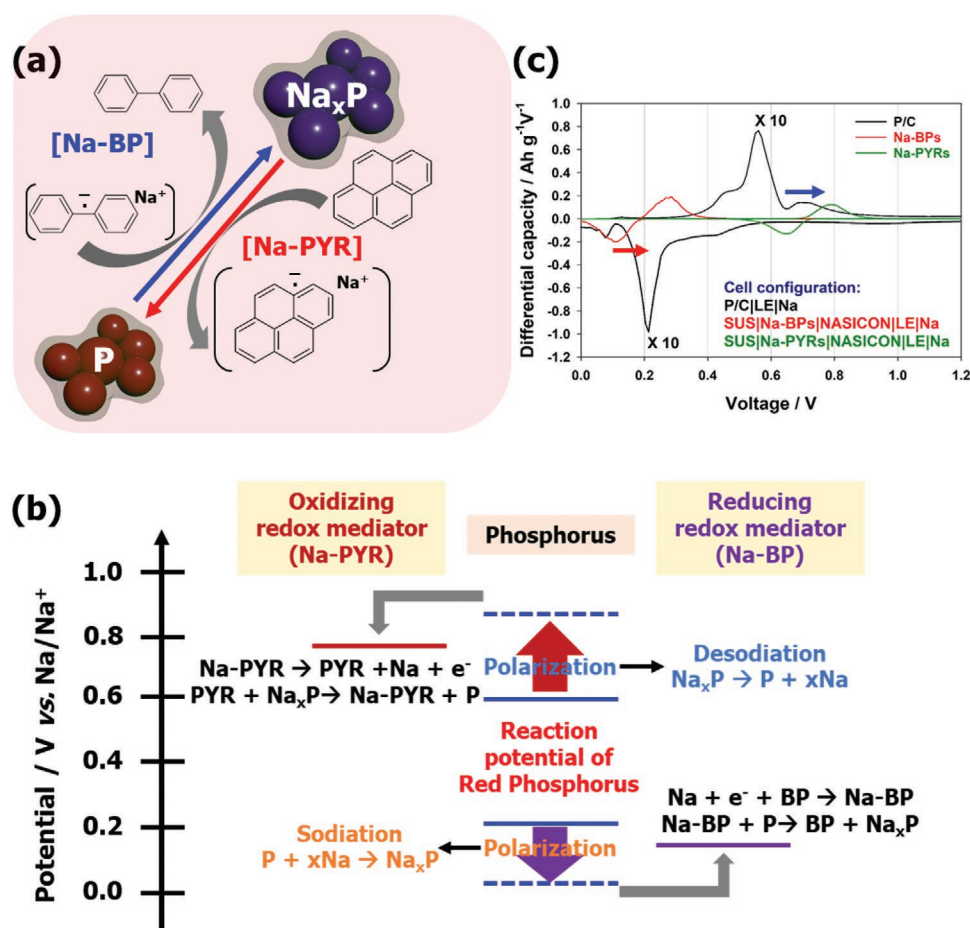


**Figure 1.** Role of redox mediators in red phosphorus semi-liquid anode. a) Reaction mechanism scheme of red phosphorus semi-liquid anode including redox mediator couples (i.e., sodium biphenyl (Na-BP) and sodium pyrene (Na-PYR)). b) Working mechanism of redox mediators (Na-BP and Na-PYR) for red phosphorus semi-liquid anode in terms of reaction potential. c) Comparing differential capacity plots of half-cells (the 5<sup>th</sup> cycle) with amorphous red phosphorus/carbon (P/C) composite foil electrode, Na-BP + 0.5 m NaPF<sub>6</sub> (Na-BPs), and Na-PYR + 0.5 m NaPF<sub>6</sub> (Na-PYRs). Liquid electrolyte (LE): 1.0 m NaPF<sub>6</sub> in DEGDM. *T* = 20 ± 3 °C.

composite (charge transfer reaction by reduction of PYR). Upon sodiation, BP is firstly sodiated (reduced). The resulting Na-BP chemically reduces the P/C composite (charge transfer reaction by oxidation of Na-BP). To confirm that the selected Na-PAHs have suitable redox potential to work in combination with the P/C composite, voltage profiles (Figure S1, Supporting Information) and differential capacity plots (Figure 1c) of half-cell with either a conventional P/C composite electrode (coated on the Al foil) or Na-PAHs anolytes including supporting electrolyte, i.e., Na-BPs (1.0 M Na-BP + 0.5 M NaPF<sub>6</sub> in DEGDME) and Na-PYRs (0.7 M Na-PYR + 0.5 M NaPF<sub>6</sub> in DEGDME), are compared in the 5<sup>th</sup> cycle. In the voltage profiles (Figure S1, Supporting Information), the main sodiation and desodiation voltages of the P/C composite are located above the sodiation voltage of Na-BP and below the desodiation voltage of Na-PYR, respectively. In fact, as displayed in the differential capacity plot (Figure 1c), the main sodiation and desodiation voltages of the P/C composite are located at about 0.21 and 0.56 V, respectively. Whereas, the sodiation voltage of Na-BP is about 0.15 V and the desodiation voltage of Na-PYR is at ca. 0.8 V (Figure 1c). In summary, the sodiation voltage of Na-BP is lower than that of the P/C composite and the desodiation voltage of Na-PYR is higher than that of the P/C composite. Therefore, these two Na-PAHs can be considered as suitable redox mediators for P/C-based anodes.

## 2.2. Conductivity of Na-PAHs

Before applying the redox mediators in the red phosphorus semi-liquid anode, the isothermal transient ionic current (ITIC) method was utilized to independently measure the ionic and electronic conductivities of Na-PAHs (see Figure S2 and Table S1, Supporting Information).<sup>[4,14,15]</sup> Both the ionic and electronic conductivities of Na-BPs and Na-PYRs are sufficiently high to ensure sodium and electron transport to the P/C composite at moderate current density. The reversible electrochemical performance of Na-BPs and Na-PYRs as well as their mixture (Na-BP-PYRs; 0.5 M Na-BP + 0.35 M Na-PYR + 0.5 M NaPF<sub>6</sub> in DEGDME) has been investigated in two-electrode half-cells. In this configuration, a NASICON solid electrolyte layer was employed to physically separate the Na-PAHs acting as active material at the working electrode compartment, and the Na metal acting as the counter electrode.<sup>[4]</sup> As evident from Figure S3 (Supporting Information), all Na-PAHs display negligible capacity during the first sodiation since they are already sodiated (see the corresponding description in the Experimental Section). However, in the subsequent charge (i.e., desodiation), capacities of 19.8 mAh g<sup>-1</sup> for Na-BPs (Figure S3a, Supporting Information), 13.8 mAh g<sup>-1</sup> for Na-PYRs (Figure S3b, Supporting Information), and 17.8 mAh g<sup>-1</sup> for Na-BP-PYRs (Figure S3c, Supporting Information) are observed, based on total weight of the Na-PAH liquids. Afterwards, all Na-PAHs show highly reversible sodiation/desodiation capacity for the subsequent 10 cycles, revealing consistent reaction voltages of each Na-PAH, especially in case of the mixed Na-BP-PYRs with characteristic reaction voltages of Na-BPs and Na-PYRs.

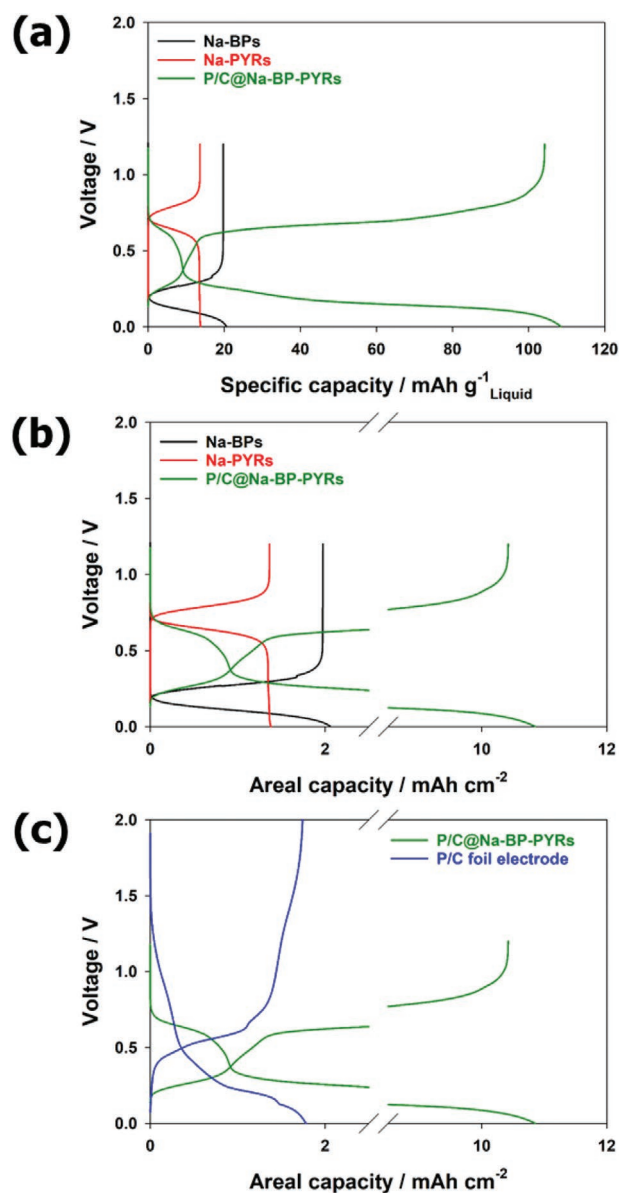


**Figure 2.** a,b) Half-cell voltage profiles in the 2<sup>nd</sup> cycle. Comparison between Na-BPs, Na-PYRs, and P/C @ Na-BP-PYRs in terms of specific (based on weight of the liquid) (a) and areal capacity (b) (current density: 0.3 mA cm<sup>-2</sup>). The half-cells are structured as follows; SUS | Working electrode | NASICON | LE | Na. Working electrode: Na-BPs, Na-PYRs, or P/C @ Na-BP-PYRs. c) Comparing the 2<sup>nd</sup> cycle voltage profiles of half-cells with P/C @ Na-BP-PYRs and P/C foil electrode. *T* = 20 ± 3 °C.

## 2.3. Red Phosphorus Semi-Liquid Anode

Following the promising performance of Na-PAHs in half-cells, a semi-liquid anode was prepared by mixing the Na-BP-PYRs and the P/C composite (hereafter referred to as P/C @ Na-BP-PYRs) and used for half-cell tests. Based on total weight of the electrode (solid + liquid), upon the 2<sup>nd</sup> cycle, the P/C @ Na-BP-PYRs anode provides much higher capacity (109 mAh g<sup>-1</sup>) than that of both Na-BPs (21 mAh g<sup>-1</sup>) and Na-PYRs (14 mAh g<sup>-1</sup>) alone (Figure 2a). As shown in Figure 2b, even in terms of areal capacity, the value obtained with

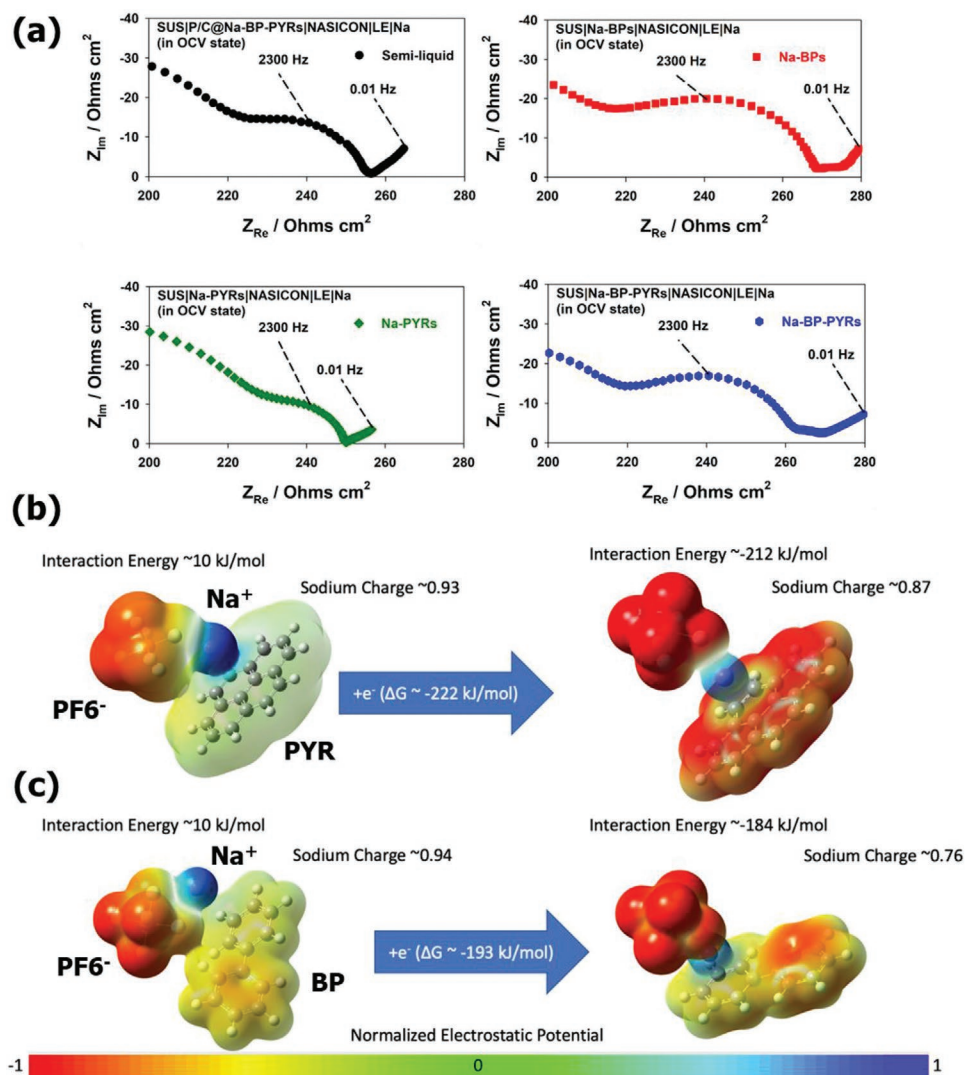


**Figure 3.** a) Electrochemical impedance spectra of half-cells in OCV state before the cycling test. The half-cells are structured as follows; SUS | Working electrode | NASICON | LE | Na. Working electrode: P/C @ Na-BP-PYRs, Na-BPs, Na-PYRs, or Na-BP-PYRs.  $T = 20 \pm 3$  °C. Density-functional theory (DFT) calculation of b) Na-PYRs and c) Na-BPs.

P/C @ Na-BP-PYRs ( $11 \text{ mAh cm}^{-2}$ ) is considerably higher than those achieved with Na-BPs ( $2.1 \text{ mAh cm}^{-2}$ ) and Na-PYRs ( $1.4 \text{ mAh cm}^{-2}$ ). When comparing with a conventional P/C electrode coated on Al foil (areal loading;  $\approx 1.5 \text{ mg cm}^{-2}$ ), the specific capacity of the P/C @ Na-BP-PYRs is lower ( $1090$  vs  $1400 \text{ mAh g}^{-1}$  for the coated electrode, see Figure S4a, Supporting Information), however, the areal capacity of the P/C @ Na-BP-PYRs is remarkably higher (see Figure 2c). In fact, such high areal capacity ( $11 \text{ mAh cm}^{-2}$ ) is very difficult to achieve with conventional coated electrodes due to their tendency to crack upon cycling (see Figure S4b, Supporting Information). The P/C @ Na-BP-PYRs provides reversible capacities of ca.  $10 \text{ mAh cm}^{-2}$  over 10 cycles, which is clearly superior to the  $1.7 \text{ mAh cm}^{-2}$  delivered by the P/C foil electrode (see Figure S4c, Supporting Information). This demonstrates the importance of developing semi-liquid anodes to increase the practical energy of battery systems. Also, electrochemical impedance spectra of semi-liquid half-cells

were collected, as shown in Figure 3a and Figure S5 (Supporting Information). It can be seen that the charge transfer resistance (especially, between the working electrode and the NASICON solid electrolyte) is smaller in case of the anolytes containing Na-PYRs. When only Na-BPs is present, the charge transfer resistance is the highest compared with Na-PYRs; P/C @ Na-BP-PYRs, Na-PYRs, and Na-BP-PYRs (Detailed explanation for the electrochemical impedance spectra is reported in the supplemental information; Figures S5–S9 and Table S2, Supporting Information). These results are also supported by density-functional theory (DFT) calculations (Figure 3b,c and Figure S8, Supporting Information), which show the sodium cation charge being higher in the case of Na-PYR (0.87, see Figure 3b) compared to Na-BP (0.76, see Figure 3c). In addition, it is clear how the reduction reaction is more favorable in the PYR-containing system with  $\Delta G = -222 \text{ kJ mol}^{-1}$  versus the BP-containing system with  $\Delta G = -193 \text{ kJ mol}^{-1}$ . Such a difference highlights that

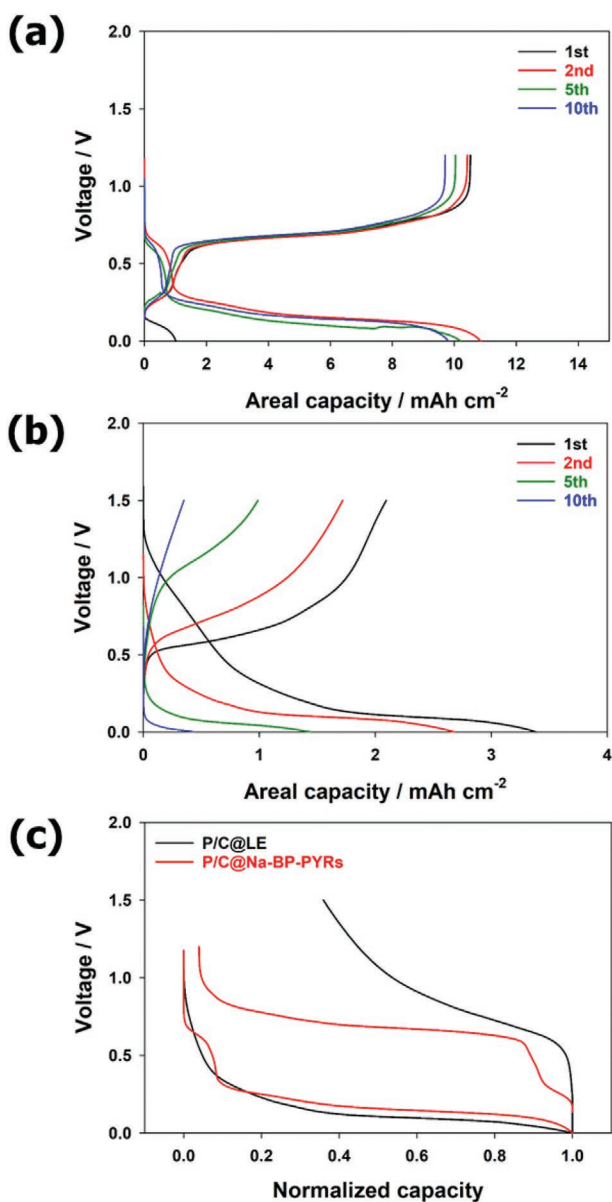


**Figure 4.** Voltage profiles of half-cells with red phosphorus semi-liquid anodes: a) P/C @ Na-BP-PYRs and b) P/C @ LE. Panel c compares the 2<sup>nd</sup> cycle voltage profiles of P/C @ Na-BP-PYRs and P/C @ LE (current density: 0.3 mA cm<sup>-2</sup>). The half-cells are structured as it follows: SUS | Working electrode | NASICON | LE | Na. Working electrodes: P/C @ Na-BP-PYRs or P/C @ LE.  $T = 20 \pm 3$  °C.

the electron is more easily accommodated in PYR since the  $\pi$  system is more extended than in BP. Even if the clear difference in energy and the electrostatic potential surfaces clearly hints to the extra electron being prominently localized on the aromatic molecules, the Natural Orbital analysis was also performed (Figure S10, Supporting Information). From that analysis, it is clearly seen how the highest occupied molecular orbital (HOMO) of the doublet systems is delocalized solely on the aromatic molecule, regardless of its nature. On this basis we can confidently say that the BP/PYR are the carrier of the negative charge.

#### 2.4. Reaction Mechanism of Red Phosphorus Semi-Liquid Anode

To comprehensively understand the reaction mechanism(s) of the P/C @ Na-BP-PYRs, a set of complementary experiments were performed, using the conventional semi-liquid anode (composed of 1 M NaPF<sub>6</sub> in DEGDMC (LE) and the P/C composite in a weight ratio of 9:1, hereafter referred to as P/C @ LE, see the corresponding description in the Experimental Section) as control sample. As it can be seen in Figure S11 (Supporting Information), the P/C @ Na-BP-PYRs delivers much higher areal capacity and improved capacity retention compared to the P/C @ LE. When comparing the voltage profiles of the two semi-liquid anodes (Figure 4), the redox mediators' role is clearly visible. As shown in Figure 4a, the P/C @ Na-BP-PYRs uptakes more than 10 mAh cm<sup>-2</sup> (based on the total semi-liquid weight of  $100 \pm 5$  mg cm<sup>-2</sup>) upon charge. This value is well retained upon the following 10 cycles. On the other hand, the P/C @ LE provides much lower charge capacity (only 2.1 mAh cm<sup>-2</sup> in the 1<sup>st</sup> cycle), which rapidly fades accompanied by severe increase in polarization (see Figure 4b). The improved reversibility and smaller polarization in the P/C @ Na-BP-PYRs can be even better appreciated comparing the 2<sup>nd</sup> cycle voltage profile for the two cells (Figure 4c).

In order to verify the working mechanism of the redox mediators, differential capacity plots and ex situ XRD analysis are combined, as shown in Figure 5. The differential capacity plots of the 2<sup>nd</sup> cycle demonstrate that the voltage profile of P/C @ Na-BP-PYRs almost overlaps those of with the reaction voltage of the Na-PAHs analytes (Figure 5a,b). During sodiation, the main peak of P/C @ Na-BP-PYRs overlaps with the one of Na-BP at about 0.11 V, while during desodiation, it overlaps with the Na-PYR peak at around 0.78 V. Also, the ex situ XRD analysis confirms the reversible reaction of phosphorus leading to mostly amorphous sodium phosphide (Figure 5c,d). The bare electrode is already sodiated, since amorphous sodium phosphide is formed during the electrode preparation. Upon desodiation, the mostly amorphous sodium phosphide disappears, but it forms again during the following sodiation. The reversibility of the process agrees with previous reports, indicating that the sodiated products are mostly amorphous, intermediate Na<sub>x</sub>P phases as a result of the limited reversible capacity accessed (around 1090 mAh g<sup>-1</sup> as shown in Figure S4a, Supporting Information).<sup>[6,7]</sup> Overall, the working mechanism of the redox mediators can be summarized in terms of energy level as depicted in Figure S12 (Supporting Information). This working mechanism is possible because the Na-PAHs analytes can exchange Na-ions and electrons, reversibly, according to their energy levels (potential).

#### 2.5. Red Phosphorus Semi-Liquid Anode in Na-SWBs

After confirming the working mechanism, P/C @ Na-BP-PYRs was tested as anode in a full Na-SWB (see Figure 6a) featuring an Ag/AgCl (3 M NaCl) reference electrode placed in the cathode compartment in order to independently follow the cathode and anode potentials.<sup>[16]</sup> As shown in Figure 6b, the potential profile of the positive electrode (seawater) displays the signature of oxygen reduction reaction (ORR) and oxygen evolution

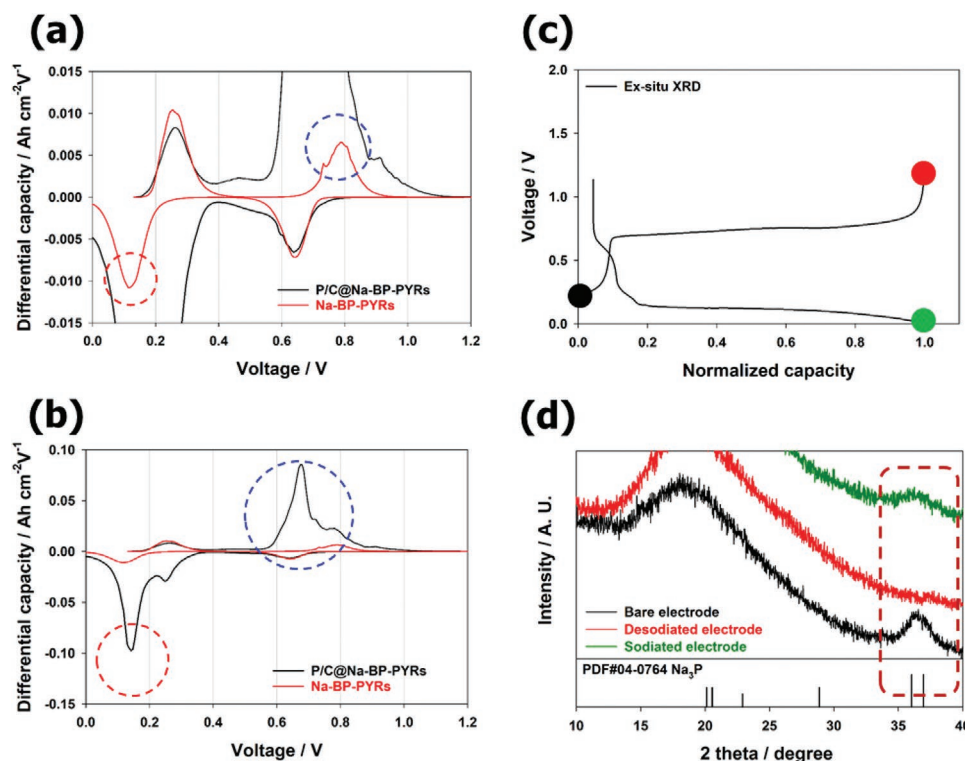


**Figure 5.** Magnified a) and overall b) differential capacity plots during the 2<sup>nd</sup> cycle of half-cell with P/C @ Na-BP-PYRs and Na-BP-PYRs. Ex situ XRD analysis of the P/C @ Na-BP-PYRs electrode. The investigated points are indicated in panel c while the XRD patterns are reported in panel d. Note that the bare electrode is already sodiated when the P/C composite is placed in contact with the sodiated redox mediators' solution.  $T = 20 \pm 3$  °C.

reaction (OER) during discharge and charge, respectively, with the operating potential ranging from 2.6 to 3.65 V.<sup>[1,17,18]</sup> The potential profile of the negative electrode (anode) evidences the reversible activity of the redox mediators, which is identical to the half-cell results previously described (see Figure 4). In summary, the electrochemical processes occurring in the Na-SWB full-cell during charge and discharge are:

Cell discharge:	Anode	Na-PYR (sol) $\rightarrow$ Na <sup>+</sup> + PYR (sol) + e <sup>-</sup> , followed by, PYR (sol) + NaP <sub>x</sub> (s) $\rightarrow$ Na-PYR (sol) + xP (s), and, Na-PYR (sol) $\rightarrow$ Na <sup>+</sup> + PYR (sol) + e <sup>-</sup>
	Cathode	2Na <sup>+</sup> + H <sub>2</sub> O + 1/2O <sub>2</sub> (g) + 2e <sup>-</sup> $\rightarrow$ 2NaOH (aq)
Cell charge:	Anode	Na <sup>+</sup> + BP (sol) + e <sup>-</sup> $\rightarrow$ Na-BP (sol), followed by, Na-BP (sol) + xP (s) $\rightarrow$ BP (sol) + NaP <sub>x</sub> (s), and, Na <sup>+</sup> + BP (sol) + e <sup>-</sup> $\rightarrow$ Na-BP (sol)
	Cathode <sup>[17,18]</sup>	2OH <sup>-</sup> (aq) $\rightarrow$ H <sub>2</sub> O + 1/2O <sub>2</sub> (g) + 2e <sup>-</sup> (+ NaClO as byproduct)

Finally, for comparison reasons, the electrochemical performance of Na-SWB full-cells employing a conventional foil anode were evaluated too (see Figure 7a). As it can be seen, during the 1<sup>st</sup> cycle, the cell displays a low coulombic efficiency around 70% due to the solid electrolyte interphase (SEI) layer formation by electrolyte decomposition. Additionally, only low areal capacities of about 2.1 mAh (= 1.0 mAh cm<sup>-2</sup>) are delivered during 10 cycles due to the limited electrode thickness. On the contrary, in case of the P/C @ Na-BP-PYRs, the presodiated

state allows for 100% coulombic efficiency in the 1<sup>st</sup> cycle and high areal capacities of around 8 mAh (= 4.0 mAh cm<sup>-2</sup>) for over 50 cycles (Figure 7b). Based on these promising results, the possibility of achieving higher reversible capacity is demonstrated using a small Na-SWB coin cell setup (Figure 8). As shown in Figure 8a,b, although the overpotential varies with the current density, the cell shows high capacities of 15 mAh (= 7.5 mAh cm<sup>-2</sup>) and exhibits stable voltage profiles over 10 cycles. Moreover, it is confirmed that, when increasing the amount of P/C @ Na-BP-PYRs (see the Experimental Section in case of higher mass loading), the cell capacity could be increased up to 30 mAh (= 15 mAh cm<sup>-2</sup>) for 5 cycles, as shown in Figure 8c.

In another test, the P/C @ Na-BP-PYRs was initially fully discharged delivering a capacity of around 26 mAh (= 13 mAh cm<sup>-2</sup>) in Figure 8d. The resulting energy densities based on total anode mass and volume are around 2200 Wh kg<sup>-1</sup> and 237 Wh L<sup>-1</sup>, respectively. After, the cell was fully recharged and then cycled at 15 mAh (= 7.5 mAh cm<sup>-2</sup>) showing good reversibility. This is an important feature of the Na-SWB system, which allows unlimited harvesting of Na-ions from seawater. For the sake of completeness, also a P/C @ Na-BP-PYRs electrode without presodiation was tested, as shown Figure S13 (Supporting Information). Finally, possible future research aspects of the P/C @ Na-BP-PYRs are depicted in Figure S14 (Supporting Information). In order to further enhance the electrochemical properties, it is certainly still necessary to increase the electronic conductivity of red phosphorus in semi-liquid state. In such a scenario, several approaches appear promising, for example designing advanced

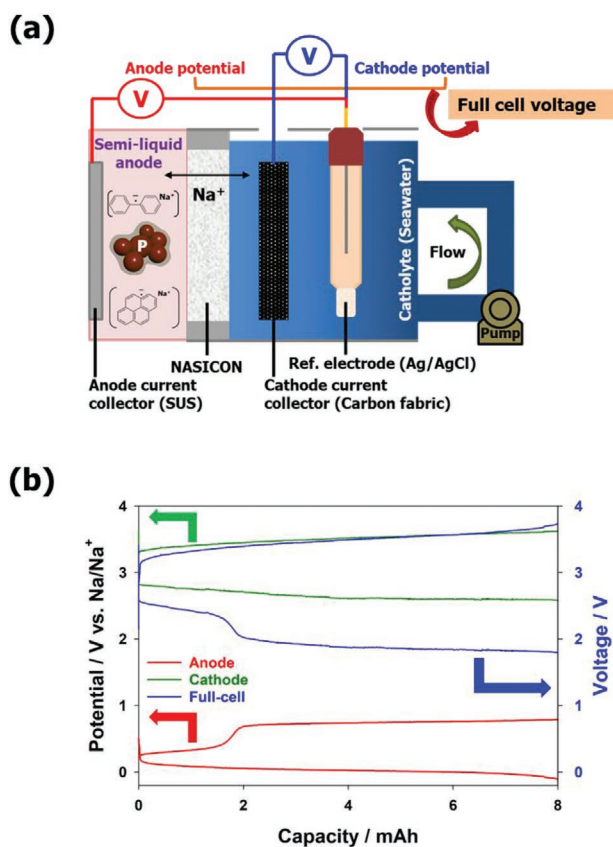


**Figure 6.** Characterization of three-electrode Na-seawater full-cell employing red phosphorus semi-liquid anode. The Ag/AgCl (3 M NaCl) reference electrode is located in the cathode compartment, as shown in (a). The charge-discharge potential profiles of each electrode as well as the full-cell voltage in the 2<sup>nd</sup> cycle (0.7 mA cm<sup>-2</sup>) are shown in (b).  $T = 20 \pm 3$  °C.

red phosphorus active materials composed of metal particles with high electronic conductivity, forming metal phosphide/phosphorus composites, as well as developing efficient current collectors with high surface area that can effectively confine the semi-liquid anode. From these points of view, energy density and cycle life are expected to be further improved.

### 3. Conclusion

A red phosphorus semi-liquid negative electrode featuring redox mediators (Na-PAHs) has been proposed for the realization of metal-free Na-seawater batteries employing the electronically insulating, but Na-ion selective solid electrolyte membrane (NASICON). The Na-PAHs anolytes (Na-BP and Na-PYR) are able to promote the de-/sodiation by acting as redox mediators for the red phosphorus active material. Remarkably, high areal capacities of around 11 mAh cm<sup>-2</sup> in Na half-cells and 15 mAh cm<sup>-2</sup> in Na-seawater full-cells could be obtained at room temperature using the semi-liquid electrode in static anode. The energy storage performance can be increased by accumulating the semi-liquid negative electrode in an external storage tank, i.e., in a full redox flow battery configuration. This

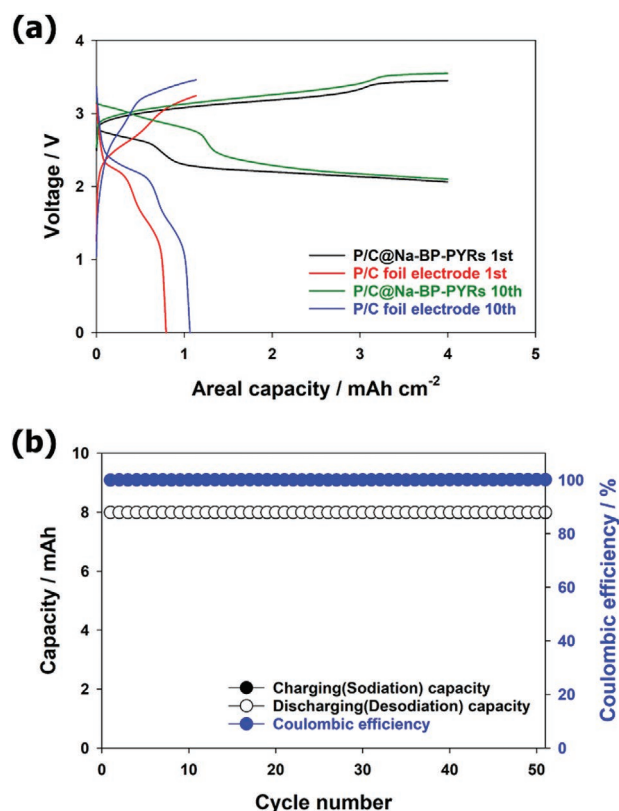


**Figure 7.** a) Voltage profiles of Na-seawater full-cells employing P/C @ Na-BP-PYRs or P/C foil electrode. b) Cyclability of a Na-seawater full-cell employing the P/C @ Na-BP-PYRs anode. Current density: 0.5 mA cm<sup>-2</sup>.  $T = 20 \pm 3$  °C.

would also allow for the continuous adjustment of the semi-liquid negative electrode compensating for degradation phenomena. These results demonstrated that the proposed system is very promising, making the Na-seawater batteries as one of the most attractive chemistries for application in large-scale stationary energy storage of the future.

### 4. Experimental Section

**Synthesis of Amorphous Red Phosphorus/Carbon composite (P/C Composite):** Amorphous red phosphorus/carbon composite powder was prepared by mechanochemical ball milling using a planetary ball milling machine (Pulverisette 6, Fritsch). The Super P carbon (Imerys, Graphite & Carbon Super P, Conductive Carbon Black) and red phosphorus (Alfa Aesar, around 100 mesh, 98.9%) at a weight ratio of 3:7 were mixed using a zirconia jar containing zirconia balls (diameter 5 mm).<sup>[7,19]</sup> The ball:powder weight ratio was 10:1. The container was filled and sealed under Ar atmosphere and the planetary ball milling was performed at 500 rpm for 24 h. Detailed characterizations of the P/C composite powders and electrodes coated on Al foil were described in a previous paper.<sup>[6]</sup>

**Preparation of Red Phosphorus Semi-Liquid Anode:** Sodium-biphenyl with supporting electrolyte (Na-BPs) and sodium-pyrene with supporting electrolyte (Na-PYRs) solutions were prepared as follows. Diethylene glycol dimethyl ether (DEGDME; Sigma-Aldrich, 99%) was dried by molecular sieve (Samchun chemical, 4 Å, 8–12 mesh) for three days to remove residual water. Subsequently, sodium hexafluorophosphate salt (NaPF<sub>6</sub>, Alfa Aesar, 99+%) was dissolved in



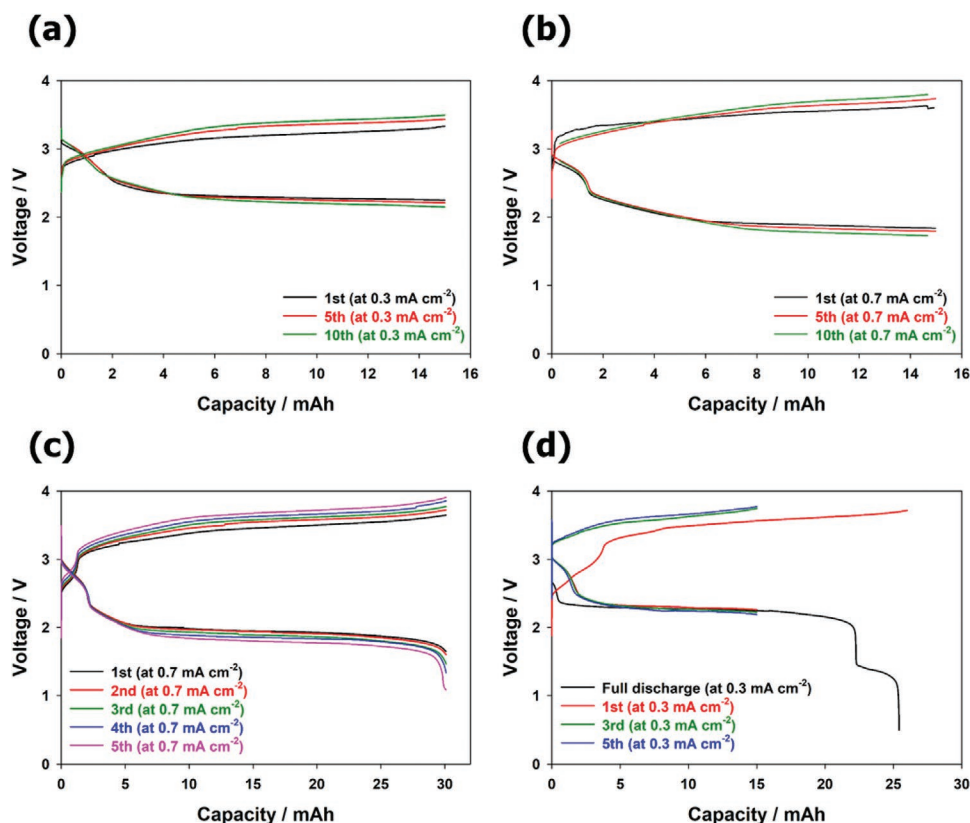


**Figure 8.** Charge-discharge voltage profiles of Na-seawater full-cells employing P/C @ Na-BP-PYRs at current densities of a) 0.3 and b) 0.7 mA cm<sup>-2</sup>, respectively (capacity: 15 mAh). c) Voltage profiles of a Na-seawater full-cell employing P/C @ Na-BP-PYRs at a current density of 0.7 mA cm<sup>-2</sup> (capacity: 30 mAh). d) Charge-discharge voltage profiles of Na-seawater full-cell employing P/C @ Na-BP-PYRs after full discharge step at a current density of 0.3 mA cm<sup>-2</sup> (nominal capacity: 15 mAh).  $T = 20 \pm 3$  °C.

the DEGDME solvent to achieve a 0.5 M concentration. Biphenyl (BP; Sigma-Aldrich, 99.5%) was added into the NaPF<sub>6</sub>-DEGDME solution achieving a 1 M concentration, which was shown to offer a rather reversible behavior in a previous study.<sup>[4]</sup> The 1 M BP-0.5 M NaPF<sub>6</sub> in DEGDME solution was stirred for 10 h. The 0.7 M PYR-0.5 M NaPF<sub>6</sub> in DEGDME solution, which is near to the saturation limit, was prepared in an analogous way using pyrene (PYR; Sigma-Aldrich, 98%). After stirring both solutions, excess sodium (Na) metal (Acros Organics, 99.8%) was added and stirred for 1 day. This step includes the charge transfer reaction leading to the formation of Na-BP and Na-PYR. The unreacted Na metal was removed from both solutions. These solutions were named as Na-BPs and Na-PYRs. To prepare the red phosphorus semi-liquid anode (P/C @ Na-BP-PYRs), Na-BPs, Na-PYRs and the P/C composite were mixed at a weight ratio of 9:9:2. Then, in order to perform sodiation of the P/C composite, excess Na metal was added and left to react for 1 day. The unreacted Na metal was removed from the red phosphorus semi-liquid anode. For comparison, a conventional liquid electrolyte-based red phosphorus semi-liquid anode (P/C @ LE) was prepared. This was composed of 1 M NaPF<sub>6</sub> in DEGDME and the P/C composite in a weight ratio of 9:1. Because each component as well as the final solutions is sensitive to water, all preparation processes were performed in a glove box with H<sub>2</sub>O and O<sub>2</sub> content of less than 1 ppm.

**Characterizations:** Electrochemical performance of the liquid anodes (including Na-BPs, Na-PYRs, and Na-BP-PYRs) and the red phosphorus semi-liquid anodes (including the P/C @ Na-BP-PYRs and the P/C @ LE) were carried out in half-cell configuration employing Na metal as counter electrode separated by a Na superionic conducting solid electrolyte (NASICON; Na<sub>3</sub>Zr<sub>2</sub>Si<sub>2</sub>PO<sub>12</sub>, obtained from 4 TO ONE Energy). The liquid anodes (Na-BPs, Na-PYRs, and Na-BP-PYRs) and

the phosphorus semi-liquid anodes (P/C @ Na-BP-PYRs and the P/C @ LE) were all tested in static conditions (no flow) using materials loadings at  $100 \pm 5$  mg cm<sup>-2</sup> of current collector (for the case of higher capacity in Na-seawater battery cell, maintaining a weight of  $150 \pm 5$  mg cm<sup>-2</sup>). For the half-cell tests employing Na metal as the counter electrode, 1 M NaPF<sub>6</sub> in DEGDME was used as the electrolyte in the counter electrode compartment. Galvanostatic cycling was conducted on a potentiostat (BCS-815, Biologic) within a potential range of 0.0–1.2 V at a current density of 0.3 mA cm<sup>-2</sup>. Isothermal transient ionic current (ITIC) measurements were conducted to separate ionic and electronic conductivity, by applying a constant voltage of 0.1 V. The resulting currents related to the ionic and electronic conductivity were measured for 1 h using a potentiostat (VSP-300, Biologic). Electrochemical impedance spectroscopy (EIS) was performed using an electrochemical interface (Solartron SI 1287, AMETEK) coupled with a frequency response analyzer (Solartron SI 1260, AMETEK) while varying the frequency from 1 MHz to 0.01 Hz with an amplitude of 10 mV. For the Na-seawater battery tests, natural seawater comprising about 0.47 M NaCl was employed as catholyte while a carbon fabric (4 × 4 cm) served as current collector. 2465-type seawater coin cells and seawater flow cell testers (supplied by 4 TO ONE Energy) were used in connection with a potentiostat (BCS-815, Biologic). Galvanostatic cycling tests were performed by charging the cells to a capacity cut-off of 4, 5, 7.5, and 15 mAh cm<sup>-2</sup>, and discharging it to a capacity cut-off of 4, 5, 7.5, and 15 mAh cm<sup>-2</sup> or voltage cut-off of 0.5 V at current densities of 0.3, 0.5, and 0.7 mA cm<sup>-2</sup>, respectively. All cells were assembled in an argon-filled glove box with less than 1 ppm of both oxygen and moisture. Ex situ X-Ray diffraction (XRD) data were collected using a Bruker AXS D8 ADVANCE apparatus with Cu-K $\alpha$  radiation ( $\lambda = 1.5405$  Å) at 40 kV and 40 mA.

**Computational Methods:** All DFT calculations were carried out using the Gaussian09 revision E software package at the B3LYP/6-311+G\* level of theory.<sup>[20]</sup> The starting geometries were hand-drawn using Avogadro and then optimized.<sup>[21]</sup> The obtained configurations were tested to be actual minima of the potential energy surface by performing a frequency calculation, and no imaginary frequency was observed. Once the singlet system was obtained in its optimized state, an electron was injected as generating a doublet system and allowed the system to relax to accommodate the extra electron. Once again, the obtained systems were tested by calculating the vibrational spectra and all the frequencies resulted positive. The energy differences were calculated using the obtained energies corrected for ZPE and accounting for the thermal correction at 298 K. The electrostatic potential surfaces were generated feeding the checkpoint file of the final frequency calculation to GaussView5.<sup>[22]</sup> The molecular orbitals were analyzed with Avogadro.

## Supporting Information

Supporting Information is available from the Wiley Online Library or from the author.

## Acknowledgements

Y.K., A.V., A.M., G.-T.K., and S.P. would like to acknowledge financial support by the Helmholtz Association.

Open access funding enabled and organized by Projekt DEAL.

## Conflict of Interest

The authors declare no conflict of interest.

## Data Availability Statement

Research data are not shared.

## Keywords

phosphorus, polycyclic aromatic hydrocarbons, redox mediators, seawater batteries, semi-liquid anodes, sodium

Received: July 6, 2021

Revised: August 12, 2021

Published online: September 1, 2021

[1] S. M. Hwang, J.-S. Park, Y. Kim, W. Go, J. Han, Y. Kim, Y. Kim, *Adv. Mater.* **2019**, *31*, 1804936.

[2] S. T. Senthilkumar, W. Go, J. Han, L. Pham Thi Thuy, K. Kishor, Y. Kim, Y. Kim, *J. Mater. Chem. A* **2019**, *7*, 22803.

- [3] M. Baumann, L. Barelli, S. Passerini, *Adv. Energy Mater.* **2020**, *10*, 2001002.
- [4] Y. Kim, J. Jung, H. Yu, G.-T. Kim, D. Jeong, D. Bresser, S. J. Kang, Y. Kim, S. Passerini, *Adv. Funct. Mater.* **2020**, *30*, 2001249.
- [5] J.-K. Kim, F. Mueller, H. Kim, D. Bresser, J.-S. Park, D.-H. Lim, G.-T. Kim, S. Passerini, Y. Kim, *NPG Asia Mater.* **2014**, *6*, 144.
- [6] Y. Kim, S. M. Hwang, H. Yu, Y. Kim, *J. Mater. Chem. A* **2018**, *6*, 3046.
- [7] Y. Kim, Y. Park, A. Choi, N.-S. Choi, J. Kim, J. Lee, J. H. Ryu, S. M. Oh, K. T. Lee, *Adv. Mater.* **2013**, *25*, 3045.
- [8] J. W. Choi, D. Aurbach, *Nat. Rev. Mater.* **2016**, *1*, 16013.
- [9] M. Duduta, B. Ho, V. C. Wood, P. Limthongkul, V. E. Brunini, W. C. Carter, Y.-M. Chiang, *Adv. Energy Mater.* **2011**, *1*, 511.
- [10] H.-D. Lim, B. Lee, Y. Zheng, J. Hong, J. Kim, H. Gwon, Y. Ko, M. Lee, K. Cho, K. Kang, *Nat. Energy* **2016**, *1*, 16066.
- [11] S. A. Freunberger, *Nat. Energy* **2016**, *1*, 16074.
- [12] G. Wang, B. Huang, D. Liu, D. Zheng, J. Harris, J. Xue, D. Qu, *J. Mater. Chem. A* **2018**, *6*, 13286.
- [13] J. Yu, Y.-S. Hu, F. Pan, Z. Zhang, Q. Wang, H. Li, X. Huang, L. Chen, *Nat. Commun.* **2017**, *8*, 14629.
- [14] H. Pan, X. Lu, X. Yu, Y.-S. Hu, H. Li, X.-Q. Yang, L. Chen, *Adv. Energy Mater.* **2013**, *3*, 1186.
- [15] G. Chu, B.-N. Liu, F. Luo, W.-J. Li, H. Lu, L.-Q. Chen, H. Li, *Chin. Phys. B* **2017**, *26*, 078201.
- [16] Y. Kim, G.-T. Kim, S. Jeong, X. Dou, C. Geng, Y. Kim, S. Passerini, *Energy Storage Mater.* **2019**, *16*, 56.
- [17] F. Dionigi, T. Reier, Z. Pawolek, M. Gliech, P. Strasser, *ChemSusChem* **2016**, *9*, 962.
- [18] N. Kim, J.-S. Park, A. M. Harzandi, K. Kishor, M. Ligaray, K. H. Cho, Y. Kim, *Desalination* **2020**, *495*, 114666.
- [19] J. Qian, X. Wu, Y. Cao, X. Ai, H. Yang, *Angew. Chem., Int. Ed.* **2013**, *52*, 4633.
- [20] M. J. Frisch, G. W. Trucks, H. B. Schlegel, G. E. Scuseria, M. A. Robb, J. R. Cheeseman, G. Scalmani, V. Barone, G. A. Petersson, H. Nakatsuji, X. Li, M. Caricato, A. V. Marenich, J. Bloino, B. G. Janesko, R. Gomperts, B. Mennucci, H. P. Hratchian, J. V. Ortiz, A. F. Izmaylov, J. L. Sonnenberg, D. Williams-Young, F. Ding, F. Lipparini, F. Egidi, J. Goings, B. Peng, A. Petrone, T. Henderson, D. Ranasinghe, V. G. Zakrzewski, J. Gao, N. Rega, G. Zheng, W. Liang, M. Hada, M. Ehara, K. Toyota, R. Fukuda, J. Hasegawa, M. Ishida, T. Nakajima, Y. Honda, O. Kitao, H. Nakai, T. Vreven, K. Throssell, J. A. Montgomery Jr., J. E. Peralta, F. Ogliaro, M. J. Bearpark, J. J. Heyd, E. N. Brothers, K. N. Kudin, V. N. Staroverov, T. A. Keith, R. Kobayashi, J. Normand, K. Raghavachari, A. P. Rendell, J. C. Burant, S. S. Iyengar, J. Tomasi, M. Cossi, J. M. Millam, M. Klene, C. Adamo, R. Cammi, J. W. Ochterski, R. L. Martin, K. Morokuma, O. Farkas, J. B. Foresman, D. J. Fox, *Gaussian 09*, Revision E. Gaussian Inc., Wallingford CT **2016**.
- [21] M. D. Hanwell, D. E. Curtis, D. C. Lonie, T. Vandermeersch, E. Zurek, G. R. Hutchison, *J. Cheminf.* **2012**, *4*, 17.
- [22] R. Dennington, T. A. Keith, J. M. Millam, *GaussView*, Semichem Inc., Shawnee Mission Version 5, KS, **2016**.